V European Conference on Computational Fluid Dynamics
ECCOMAS CFD 2010
J. C. F. Pereira and A. Sequeira (Eds)
Lisbon, Portugal, 14–17 June 2010

AN ELEMENT-BASED FINITE VOLUME METHOD FOR SOLID MECHANICS PROBLEMS

Gerson Filippini[*], Clovis R. Maliska[†], Miguel Vaz Jr[††]

[*]Federal Technological University of Paraná,
Av. Brazil, 4232, 85884-000 Medianeira, PR, Brazil
e-mail: GFilippini@utfpr.edu.br

[†]Dept. of Mechanical Engineering, Federal University of Santa Catarina – Computational Fluid Dynamics Laboratory – SINMEC,
88040-900 - Florianopolis, SC, Brazil.
e-mail: maliska@sinmec.ufsc.br

[††]Department of Mechanical Engineering, Centre for Technological Sciences, State University of Santa Catarina, UDESC,
Campus Universitário Prof. Avelino Marcante, 89223-100 Joinville, Brazil
e-mail: M.Vaz@joinville.udesc.br

Key words: Finite Volume Method, Plane Elasticity, Fluid-Structure Interaction.

Abstract. *Recently, in terms of investigation and in a minor scale for the solution of structural mechanics problems, Finite Volume (FV) techniques has been frequently considered [1]. Recently, finite volume methods has been tested in several structural problems, such as elasticity [3,5,6], thermo-elasticity [4], visco-plasticity [7], axi-symmetric structures [8.12], incompressible materials [10.11], plates [9], orthotropy [13], welding process [15], fluid-structure interaction [14], extrusion and forging [16], among others. The results were always very promising, since the method demonstrated to be robust and always following consistently the reference solutions available, considering both, the primitive variables (displacements) and recovered variables (stresses) [2,17]. Besides its inherent robustness due to its conservative approach, another strong factor that favors the advancement of the method has been its ability in dealing with complex geometries using meshes similar to the ones used by finite element methods (FEM). But, it seems that the most promising application is its use in coupled problems, like in fluid-structure interaction, in which the same grid can be used for both problems. This paper presents the development of an Element-based Finite Volume Method (EbFVM) applied for the solution of some structural problems aiming its validation, including an order of error analysis of Richardson [2], the solution of the Patch Tests [31] and an analysis of convergence by using iterative methods for solving the linear system. The results agree well with the available results in the literature and*

encourage further development of this method for solving structural problems especially in coupled problems.

1 INTRODUCTION

The development of numerical techniques for the solution of solid and fluid mechanics problems followed two independent routes for more than two decades. Probably the nature of the governing equations and the complexity of the domain dictate the choice of the method. Finite element techniques (FEM), due to its ability in dealing with arbitrary domains and its less complex mathematical models for elasticity problems, was the choice in the solid mechanics area. In the other hand, developers of finite volume methods (FVM) were dedicated to cope with the high nonlinearities and the coupling of the fluid flow equations, and practically none was done in this area until the 80's to extend the methods to arbitrary geometries. In the last two decades finite element developers extended their techniques to solve problems in almost all areas, while the finite volume methods were extended to deal with arbitrary geometries and unstructured meshes, becoming extremely powerful and a largely used tool for fluid mechanics problems, the well known CFD area.

Attempting to the extensions of the FEM and FVM methodologies to solve other class of problems, one realize that strong efforts were dedicated in the FEM area for adapting their techniques for solving fluid mechanics problems. The opposite is not true, and less effort was dedicated to apply the FVM technologies to solid mechanics problems. Based on the fact that FVM has abilities for solving the full momentum conservation equations, why are those techniques not extensively applied to solve solid mechanics problems? This is the scope of this paper, in which and Element-based Finite Volume Method (EbFVM) is extended to deal with elasticity problems. This method borrows from the finite element techniques all the geometric definitions and strategies, including the sweeping of the domain for the matrix assembling. The main difference among FVM and FEM is in obtaining the approximate equations. The former does the task through balances of the transported physical quantities over control volumes created based on the elements, while the former does not have the concept of volume conservation implied.

Since engineering presses for more general techniques for solving coupled problems in several areas, one foresees that the EbFVM techniques can be successfully applied to those problems by using the same mesh and the same robust approximation offered by the finite volume procedures. Even when the coupled domains are solved sequentially, the transfer of information among domains easily transferred if the grids are of the same nature. The following statement, found in Slone et al. [14], explain the requirements when solving a coupled problem:

"*Unless the fluid-structure coupling is either one way, very weak or both, transferring and filtering data from one mesh and solution procedure to another may lead to significant problems in computational convergence. It becomes clear that when addressing dynamic fluid-structure interaction problems, for those with any significant degree of coupling, the solution procedures in the solid and fluid domains have to be compatible in respect of:*

- *The mesh structure and element order;*
- *The method of spatial discretization;*

- *The two-way exchange of information of the fluid-structure interface."*

With this major motivation in mind, this paper describes a EbFVM technique successfully employed for CFD problems, for the solution of solid mechanics problems. The main goal is the presentation and evaluation the method using well-known test problems found in the literature.

1.1 Developments - Historical View

This section tries to list in chronological order, the major developments made in extending FVM techniques to solid mechanics problems. In 1964 Wilkins *apud* Zienkiewicz [18] can be regarded as introducing the FVM in the structural field. After some dormant period, in 1991 Fryer *et al.* [3] returned to the topic with the work: *A Control Volume Procedure for Solving the Elastic Stress-Strain Equations on an Unstructured Mesh*. In 1992 Lahrmann [19] presented a work where the formulation for FV is discussed for complex geometries, and in 1994 Idelsohn and Oñate [20] published their *Finite Volumes and Finite Elements: Two "Good Friends"*, a paper with brought to the field an open view of the problem. In 1994 Onãte, Cervera and Zienkiewicz [5] presented a formulation for structural mechanics also applicable to complex geometries. In 1995 Bailey and Cross [6] published an extension of the work of Fryer *et al.* [3] using finite volumes for solving problems of elasticity in 3D unstructured grids. In same year, Taylor, Bailey and Cross [7] applied FV for elasticity problems considering visco-plasticity. Following, in 1996, Whell [8] presented an approach for axi-symmetric structures and Fainberg and Leister [4], applied FV and the multigrid technique in a thermo-elasticity problem for anisotropic materials. In 1997 Bailey et al. [21] modeled the solidification of metals and Wheel [9] presented a formulation for plates. Again Wheel, in 1997 and 1998 [10,11] presented the modeling of incompressible materials using a mixed approach. In 1999 Taylor, Bailey and Cross [22] offered a formulation using an elastic-plastic model for small deformations.

In 2000 Fallah *et al.* [23] presented a comparison between FVM and FEM for nonlinear stress analysis problem. In same year Zarrabi and Basu [12], using a Cell-centered Finite Volume Method (CC-FV) solved of elasticity problems for axi-symmetric domains, and Demirdžić, Horman and Martinović [13] published the formulation in CC-FV to a orthotropic material. It considers that deformations happen not only due to the imposition of displacement and/or required force, but also due to the presence of temperature and moisture. In 2002, the range of applications increased with Yamamoto, Fang and Tsuchiya [24] realizing a comparison between the FDM, FEM and FVM for a one-dimensional problem, Slone *et al.* [14] solved a problem of fluid structure iteration, Taylor *et al.* [15] solved a welding problem using FV and Williams, Croft and Cross [16] simulated the processes of extrusion and forging of metals. In 2003 Wheel and Wenke [25] presented a FV method which incorporated a degree of freedom for rotation and Slone, Bailey and Cross [26] a formulation applied to the dynamics of solids for small deformations including viscous damping. In 2004 Filippini [17] applied FVM to plane elasticity in isotropic material, comparing key situations with FEM, especially when spurious modes are presented in the solution using MEF. In 2007 Xia *et al.* [27] solved a elastic 3D problem using FVM implicit in time, Zhao *et al.* [28] employing an implicit formulation in time with unstructured meshes using FV for both solid and the fluid flow problem. Again in 2007, Limache and Idelsohn [29] emphasized that using FVM techniques is a very interesting route for solving solid mechanics

problems, listing several factor for this choice. Finally, in 2009 Vaz Jr, Muñoz-Rojas and Filippini [2], presented an analysis of errors in the calculation of node stresses using the finite volume and finite element methods.

These citations comprise much of the work in the area. An overall evaluation of the results reported has been very positive, motivating the use of finite volume techniques in these types of problems. Some of the characteristics of the method deserve to be highlighted:

- The good convergence and stability of the numerical solution;
- Ease of implementation in existing computational algorithms for fluid flow;
- Facilitates the exchanging of information among the domains involved;
- The strict conservation of physical quantities at the discrete control volume level means that one is respecting what the point-level partial differential equations requires. It must be always recalled that the partial differential equations represents a point-level balance of the physical quantities. The finite volume approximation equations are merely one of steps in the process of deriving any equation governing a physical phenomenon.

2 EQUILIBRIUM EQUATIONS AND CONSTITUTIVE RELATIONS

The equilibrium equations are obtained by applying the linear and angular momentum equations to a differential volume, obtaining

$$\begin{cases} \operatorname{div}[\boldsymbol{\sigma}] + \mathbf{b} = \rho \ddot{\mathbf{u}} \\ \boldsymbol{\sigma} = \boldsymbol{\sigma}^{\mathrm{T}} \end{cases} \text{ with } \begin{cases} \mathbf{u} = \bar{\mathbf{u}} & \mathbf{x} \in \partial\Omega^{\mathrm{u}} \\ \boldsymbol{\sigma}\mathbf{n} = \bar{\mathbf{t}} & \mathbf{x} \in \partial\Omega^{\mathrm{t}} \end{cases} \text{ with } \begin{cases} \partial\Omega = \partial\Omega^{\mathrm{u}} \cup \partial\Omega^{\mathrm{t}} \\ \partial\Omega^{\mathrm{u}} \cap \partial\Omega^{\mathrm{t}} = \varnothing \end{cases} \tag{1}$$

where $\boldsymbol{\sigma}$ is the stress tensor, $\mathbf{b}$ the body forces, $\ddot{\mathbf{u}}$ the acceleration and ρ the specific mass. The boundary conditions are defined so that $\mathbf{n}$ is the outward normal unit vector and $\bar{\mathbf{u}}$ and $\bar{\mathbf{t}}$ are prescribed displacements and loads, respectively. Quasi-static deformation is assumed in the present work (no inertia effects are accounted for).

The constitutive relation for linear elastic solids is well known in the literature, in which, for sufficiently small deviations from a given reference state, the stress-strain relation is known as *generalized Hooke´s law*,

$$\boldsymbol{\sigma} = \boldsymbol{\sigma}_0 + \mathbf{D} : \boldsymbol{\varepsilon}^e \quad \text{and} \quad \boldsymbol{\varepsilon}^e = \frac{1}{E}\left[(1+\nu)\boldsymbol{\sigma} - \nu \operatorname{tr}(\boldsymbol{\varepsilon})\mathbf{I}\right] \tag{2}$$

in which $\boldsymbol{\sigma}_0$ is the initial stress tensor, $\mathbf{D}$ is the isothermal elastic modulus, $\boldsymbol{\varepsilon}^{\mathrm{e}}$ the elastic strain tensor, E the Young modulus, ν the Poisson´s ratio and $\boldsymbol{I}$ denotes the second order identity tensor. Equations for plane stress and plane strain problems can be readily derived from Eq. (2), which, in terms of stress and strain components is,

$$\begin{Bmatrix} \sigma_{xx} \\ \sigma_{yy} \\ \sigma_{xy} \end{Bmatrix} = A \begin{bmatrix} a & b & 0 \\ b & a & 0 \\ 0 & 0 & c \end{bmatrix} \begin{Bmatrix} \varepsilon_{xx} \\ \varepsilon_{yy} \\ 2\varepsilon_{xy} \end{Bmatrix} \tag{3}$$

in which the constants of Eq. (3) are given in Tab. 1.

	1D	EPT	EPD	3D
D	1	2		3
A	E	$\frac{E}{1-\nu^2}$	$\frac{E}{(1+\nu)(1-2\nu)}$	
a	1	1	$1-\nu$	1
b	0	ν	ν	ν
C	$C=\frac{a+(1-D)b}{2}$			

Table 1: Constants of Eq.(3)

where $\varepsilon_{xx} = \partial u/\partial x$, $\varepsilon_{yy} = \partial v/\partial y$ and $2\varepsilon_{xy} = \gamma_{xy} = (\partial u/\partial y + \partial v/\partial x)$, are the strain components, and u and v are displacements along the *x* and *y* directions, respectively.

3 FINITE VOLUME APPLIED TO PLAIN ELASTICITY

The mathematical concept of the finite volume method is very simple and basically consists on the application of the equilibrium equations to discrete, non-overlapping controls volumes. The literature shows several different strategies to discretize the governing equations using finite volume techniques. They can be cast into two major categories: cell-vertex and cell-centered schemes. This work uses a cell-vertex scheme, named herein Element-based Finite Volume Method (EbFVM), employing unstructured grids comprising triangular or quadrilateral elements, or both. In the literature this method is often called Control Volume Finite Element Method (CVFEM). One avoids this denomination because it conveys to the reader the wrong idea that CVFEM is a Finite Element Method which uses the control volume. In fact, it is a Finite Volume Method which uses the element.

3.1 The Element and the Control-Volume

The element is the primary geometrical entity of the method and Fig.1 presents the construction of the finite volume method based on the elements, by joining the center of the elements to its mid-face around a specific node. In this construction the center of the control volume is a vertex of the element, therefore, it is a cell-vertex method.

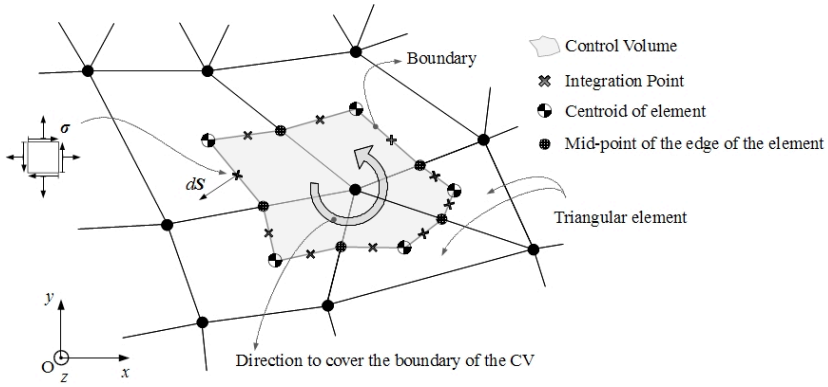

Figure 1: Construction of the control volume.

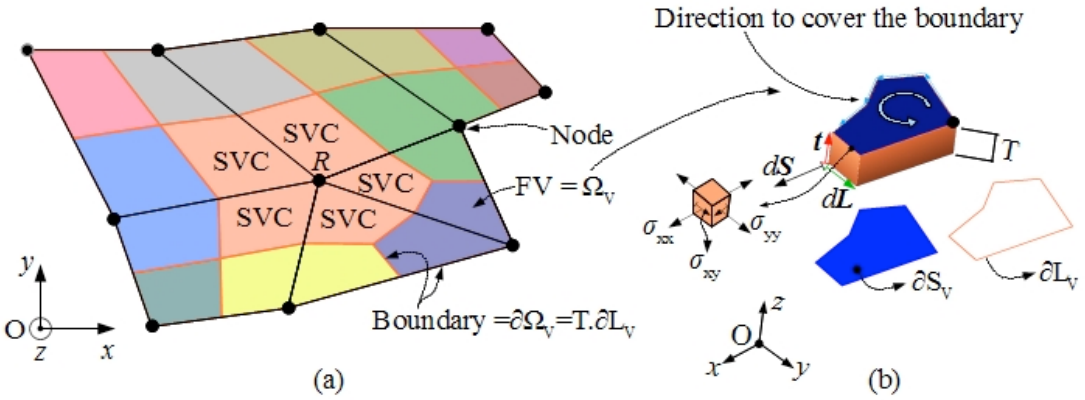

Figure 2: 2D discretization with thickness T (a) and Vectors for one face of a control volume (b)

Fig.2(a) shows a discretization where triangular and quadrilateral elements are present with a control volume created using parts of the five surrounding elements, and a Fig.(2b) shows the sweeping direction of the boundary, the constant thickness vector, ($\boldsymbol{t} = [0,0,T]^{T}$), the border vector ($\boldsymbol{L}$) and the surface vector ($\boldsymbol{S}$), where $\boldsymbol{S} = \boldsymbol{L} \times \boldsymbol{t}$.

3.2 The finite volume equilibrium equation

The general discretization procedure is summarized as follows: Firstly, the linear equilibrium equation, Eq. (1), in its conservative form is integrated over the control volume, followed by application of the divergence theorem, resulting in

$$\iiint_{\Omega_V} \mathrm{div}[\boldsymbol{\sigma}]d\Omega + \iiint_{\Omega_V} \mathbf{b}d\Omega = \iint_{\partial\Omega_V} \boldsymbol{\sigma}d\mathbf{S} + \iiint_{\Omega_V} \mathbf{b}d\Omega = \mathbf{0} \tag{3}$$

where $d\mathbf{S}$ is the differential vector of the volume surface ($\partial\Omega_V$), Ω_V is the control volume and $d\Omega$ its respective elemental volume. Substituting the 3D stress tensor and its corresponding vectors, one gets

$$\oint_{\partial L_V} \begin{bmatrix} \sigma_{xx} & \sigma_{xy} & 0 \\ \sigma_{yx} & \sigma_{yy} & 0 \\ 0 & 0 & \sigma_{zz} \end{bmatrix} \begin{vmatrix} \mathbf{i} & \mathbf{j} & \mathbf{k} \\ dL_x & dL_y & 0 \\ 0 & 0 & T \end{vmatrix} + \iiint_{\Omega_V} \begin{Bmatrix} b_x \\ b_y \\ 0 \end{Bmatrix} d\Omega = \begin{Bmatrix} 0 \\ 0 \end{Bmatrix} \tag{4}$$

where $d\mathbf{S}$ was substituted by its respective vector product. For the 2D analysis carried out in this work the resulting equation for a plane state of tension is

$$\oint_{\partial L_V} \begin{bmatrix} \sigma_{xx} & \sigma_{xy} & 0 \\ \sigma_{yx} & \sigma_{yy} & 0 \\ 0 & 0 & \sigma_{zz} \end{bmatrix} \begin{Bmatrix} dL_y.T \\ -dL_x.T \\ 0 \end{Bmatrix} + \iiint_{\Omega_V} \begin{Bmatrix} b_x \\ b_y \\ 0 \end{Bmatrix} d\Omega = T \oint_{\partial L_V} \begin{Bmatrix} \sigma_{xx}dL_y - \sigma_{xy}dL_x \\ \sigma_{yx}dL_y - \sigma_{yy}dL_x \\ 0 \end{Bmatrix} + \iiint_{\Omega_V} \begin{Bmatrix} b_x \\ b_y \\ 0 \end{Bmatrix} d\Omega = \mathbf{0} \tag{5}$$

Representing dL_x and dL_y by dx and dy, *one gets*

$$\oint_{\partial L_V} \begin{Bmatrix} \sigma_{xx}dy - \sigma_{xy}dx \\ \sigma_{yx}dy - \sigma_{yy}dx \end{Bmatrix} + \iint_{\partial S_V} \begin{Bmatrix} b_x \\ b_y \end{Bmatrix} dxdy = \begin{Bmatrix} 0 \\ 0 \end{Bmatrix} \tag{6}$$

Substituting the deformations and their relations, one gets

$$\oint_{\partial L_V} A \begin{Bmatrix} \left(a\dfrac{du}{dx}+b\dfrac{dv}{dy}\right)dy-c\left(\dfrac{dv}{dx}+\dfrac{du}{dy}\right)dx \\ c\left(\dfrac{dv}{dx}+\dfrac{du}{dy}\right)dy-\left(b\dfrac{du}{dx}+a\dfrac{dv}{dy}\right)dx \end{Bmatrix} + \iint_{\partial S_V} \begin{Bmatrix} b_x \\ b_y \end{Bmatrix} dxdy = \begin{Bmatrix} 0 \\ 0 \end{Bmatrix} \tag{7}$$

3.3 Parametric element. Coordinate transformation

In order to generalize and facilitate the computational process of integration, that is, the coefficients calculation and assemble of the global matrix, it is convenient to parameterize the variables *x* and *y* or, in other words, to have a transformed element with parametric coordinates (local coordinates). In this study, only quadrilateral elements are used, although all the formulation holds for other type of elements. The parameterization is shown in Fig. 3, with the element in *(x,y)* global coordinate system, Fig.3(a), and in Fig. 3(b) in the local coordinate system, *(r,s)*. The shape functions and the mathematical relations derived from the transformation are given by

$$\begin{aligned}
&N_1 = \tfrac{1}{4}(1+r)(1+s) \quad N_3 = \tfrac{1}{4}(1-r)(1-s) \\
&N_2 = \tfrac{1}{4}(1-r)(1+s) \quad N_4 = \tfrac{1}{4}(1+r)(1-s) \\
&\phi\ (r;s) = N_1\phi_1 + N_2\phi_2 + N_3\phi_3 + N_4\phi_4 \\
&J(r,s) = \frac{\partial x}{\partial r}\frac{\partial y}{\partial s} - \frac{\partial x}{\partial s}\frac{\partial y}{\partial r} \\
&dxdy = J\,drds \\
&dx = \frac{\partial x}{\partial r}dr + \frac{\partial x}{\partial s}ds, \quad dy = \frac{\partial y}{\partial r}dr + \frac{\partial y}{\partial s}ds
\end{aligned}
\qquad
\begin{aligned}
&\frac{\partial \phi}{\partial r} = \frac{\partial N_i}{\partial r}\phi_i \quad e \quad \frac{\partial \phi}{\partial s} = \frac{\partial N_i}{\partial s}\phi_i \\
&\frac{\partial \phi}{\partial x} = J\left(\frac{\partial N_i}{\partial r}\frac{\partial y}{\partial s}\phi_i - \frac{\partial N_i}{\partial s}\frac{\partial y}{\partial r}\phi_i\right) \\
&\frac{\partial \phi}{\partial y} = J\left(\frac{\partial N_i}{\partial s}\frac{\partial x}{\partial r}\phi_i - \frac{\partial N_i}{\partial r}\frac{\partial x}{\partial s}\phi_i\right) \\
&Para\ i = 1...4
\end{aligned}
\tag{8}$$

in which N_i and ϕ_i are values associated with the i^{th} local node, ϕ can be any variable within the domain of the element, and *J* represents the *Jacobian* of the transformation.

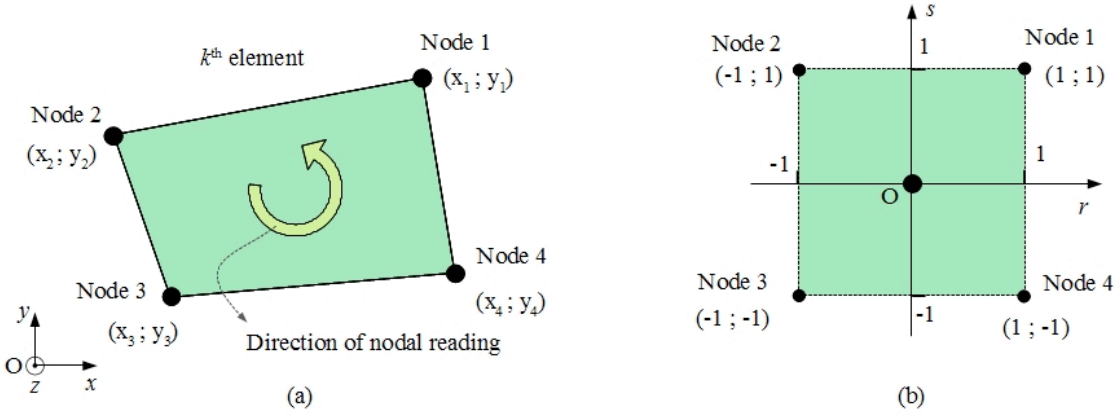

Figure 3: Element in global coordinates (a), and local coordinates (b).

3.4 The discrete finite volume equations in local coordinates

As can be seen in Fig 2(a), the control volume R, for example, is formed assembling parts of the elements, called sub-control volumes (SVC), sharing the same node. The integration along the boundary ∂L_V is performed in the faces of each SVC, that is, two integration points exist for each SVC, one in each face, named f_1 and f_2 (see, for instance, Figs. 4(a) and 4(b).

Although the discretization is performed using balances over a control volume, the computational code will sweep element-by-element assembling the equation for a specified control volume. All information are stored at the element. For example, in a 2D case, for a quadrilateral element, 8 integration points will be known for each element. At those integration points fluxes will be calculated and stored. When assembling the global matrix, 2 of these fluxes of each element will be used for constructing the approximate equation for that control volume.

These faces (f_1 and f_2) are generalized through the line f_m shown in Fig. 4(c), considering the **position** of the Integration Point (*IP*), and the sweeping **direction** of the control volume border. Considering linear variation at the faces, the Gauss-Legendre integration with one integration point suffices to obtain the exact integral of the polynomial. The integrations points IP_1 and IP_2 are shown in Figs. 4(a) and 4(b) in the global and transformed coordinate system, respectively.

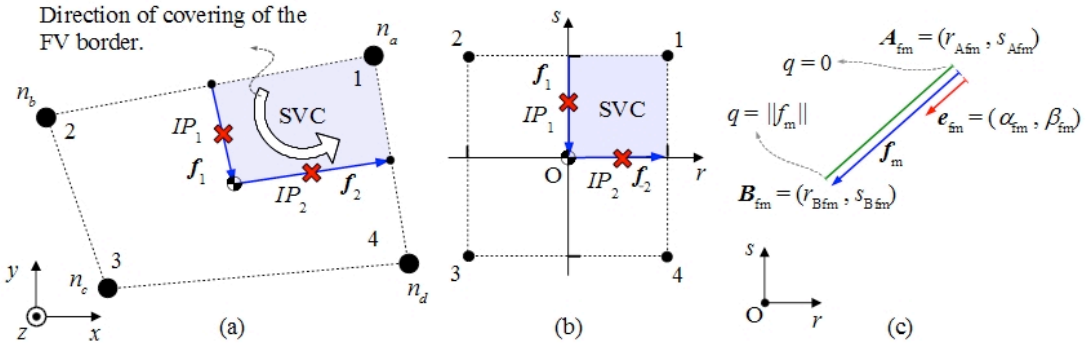

Figure 4: Integrations points in the faces of a SVC, (a) and (b). Generic face $\boldsymbol{f}_m=\boldsymbol{B}_{fm}-\boldsymbol{A}_{fm}$, unity vector $\boldsymbol{e}_{fm}=(\alpha_{fm};\beta_{fm})$ and parametric variable q (c)

Using the expressions given in Eq. (8), one obtains

$$A \oint_{\partial L_{V_{lk}}} \left\{ b\, u_a^m\, N_{a'm}\, \delta_{ij} + C\left(u_a^i\, N_{a'j} + u_a^j\, N_{a'i} \right) \right\} \varepsilon_{jnp} e_p dx_n = g_i^e \quad \text{onde} \quad g_i^e = -\iint_{\partial S_{V_{lk}}} b_i\, e \, \mathrm{d}x\mathrm{d}y$$

$$i = 1..2, \quad j = 1..2, \quad a = 1..4, \quad m = 1..2, \quad n = 1..3, \qquad (9)$$

$$p = 1..3, \quad l = 1..4, \quad k = 1..n_{elem}$$

Eq. (9) for a quadrilateral element has 8 equations and 8 unknowns values [u_{na}, v_{na}, u_{nb}, v_{nb}, u_{nc}, v_{nc}, u_{nd}, v_{nd}]^T which are the nodal displacements of the element. A, b and C appearing in Eq.(9) are defined in the Tab.1, and u_a^m, u_a^i, u_a^j are the displacements of a node a in the direction defined by m, i and j, respectively. $N_{a'm}$, $N_{a'i}$, $N_{a'j}$ are the derivatives of the a^{th} shape function in relation to the directions m, i or j, and, δ_{ij} is the

Kronecker Delta, ε_{jnp} is the alternating tensor, e_p is the thickness vector, where p indicates one of the main directions, dx_n indicates the differential length (dx and dy) and g_i^s are the body forces integrated over the SVC. To conclude the definitions, i and j are free indexes indicating rows and columns in the matrix. By its turn, l is an index, and will generate a new system for each value of l. This in fact indicates the node that is associated with the SVC and k indicates the element. The relations,

$$\begin{cases} r = r_{Afm} + \alpha_{fm} q \\ s = s_{Afm} + \beta_{fm} q \end{cases} \qquad \begin{cases} \alpha_{fm} = \dfrac{r_{Bfm} - r_{Afm}}{\|\mathbf{f}_m\|} \\ \beta_{fm} = \dfrac{s_{Bfm} - s_{Afm}}{\|\mathbf{f}_m\|} \end{cases} \qquad \begin{cases} \mathrm{d}r = \alpha_{fm} \mathrm{d}q \\ \mathrm{d}s = \beta_{fm} \mathrm{d}q \end{cases} \tag{10}$$

are used to obtain

$$\left(\begin{array}{l} T A \sum_{m=1}^{2} \left\{ \int_0^1 \left[\left((b+2C) y_{,r} N_{i'x} - C x_{,r} N_{i'y} \right) \alpha_{fm} + \left((b+2C) y_{,s} N_{i'x} - C x_{,s} N_{i'y} \right) \beta_{fm} \right] dq \right\} u_i + \\ \quad T A \sum_{m=1}^{2} \left\{ \int_0^1 \left[\left(-C x_{,r} N_{i'x} + b y_{,r} N_{i'y} \right) \alpha_{fm} + \left(-C x_{,s} N_{i'x} + b y_{,s} N_{i'y} \right) \beta_{fm} \right] dq \right\} \mathrm{v}_i = g_x^e \\ T A \sum_{m=1}^{2} \left\{ \int_0^1 \left[\left(-b x_{,r} N_{i'x} + C y_{,r} N_{i'y} \right) \alpha_{fm} + \left(-b x_{,s} N_{i'x} + C y_{,s} N_{i'y} \right) \beta_{fm} \right] dq \right\} u_i + \\ \quad T A \sum_{m=1}^{2} \left\{ \int_0^1 \left[\left(C y_{,r} N_{i'x} - (b+2C) x_{,r} N_{i'y} \right) \alpha_{fm} + \left(C y_{,s} N_{i'x} - (b+2C) x_{,s} N_{i'y} \right) \beta_{fm} \right] dq \right\} \mathrm{v}_i = g_y^e \end{array} \right)_{j\,k} \tag{11}$$

Eq. (11) refers to a system for a SVC associated to a particular element, that is, has the relationship between the eight displacements $[u_{na}, \mathrm{v}_{na}, u_{nb}, \mathrm{v}_{nb}, u_{nc}, \mathrm{v}_{nc}, u_{nd}, \mathrm{v}_{nd}]^T$. However, starting with Eq. (11) for a j^{th} SVC in some k^{th} element, we can define a **nodal matrix** that relates the i^{th} **local node** to a j^{th} **SVC**. This matrix appears in the nodal equation, Eq.(12), represented as K_{ij}^n where n indicates nodal matrix. The components of K_{ij}^n are the respective multipliers in terms of u_i and v_i of Eq. (11).

$$\left(\sum_{i=1}^{n_{psl}} \left(\begin{bmatrix} K_{xu}^n & K_{x\mathrm{v}}^n \\ K_{yu}^n & K_{y\mathrm{v}}^n \end{bmatrix} \begin{Bmatrix} u_i \\ \mathrm{v}_i \end{Bmatrix} \right) = \begin{Bmatrix} g_x^e \\ g_y^e \end{Bmatrix} \right)_{j\,k} \tag{12}$$

3.5 Assembly of the equations system

The final system equations has the following form

$$\mathbf{K}\mathbf{u}^* = \mathbf{g} \tag{13}$$

in which $\mathbf{u}^*$ is the solution vector, $\mathbf{K}$ is the stiffness matrix and $\mathbf{g}$ the forcing vector. To assemble $\mathbf{K}$ is necessary sweep the domain for each k^{th} element locating the matrix as

K_{ij}^n present in Eq. (12) for each j^{th} SVC and each i^{th} element node, placing the components as K_{ij}^n in their positions with the help of the matrix connectivity. This process is illustrated in Fig. 5.

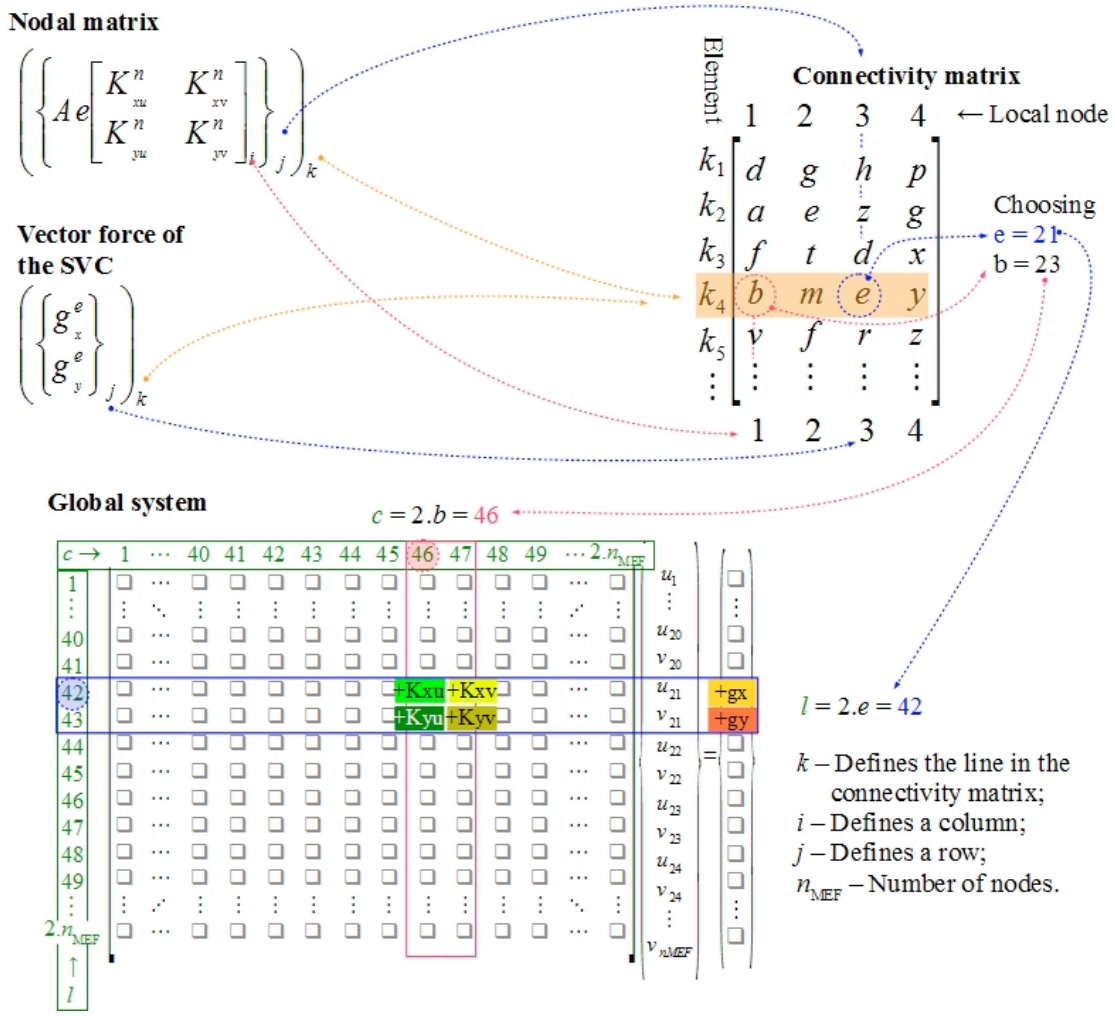

Figure 5: Assembly of the equations system from the nodal matrix, forcing vector and connectivity matrix.

4 TEST CASES

The main goal os this section is to apply the developed method to some well-known problems such that the computer implementation and basic behaviors of the method can be checked. There is no interest in solving complex solid mechanics problems at this moment, target to be done in a next paper.

4.1 Richardson extrapolation

Since it is impossible to reach zero size for the mesh, *Richardson extrapolation* [2] was conceived for extrapolating finite size mesh solutions to get the "exact" solution, φ_{exact}, at a given point, by

$$\varphi_{exact}(\mathbf{x}) = \varphi_h(\mathbf{x}) + e_h(\mathbf{x}) = \varphi_h(\mathbf{x}) + M\,h^p + O(h^{p+1}) \tag{14}$$

where φ_h is the discrete solution, e_h is the approximation error, h is the mesh size, M is a constant and p is the local error order. A safe application of the Richardson extrapolation requires three assumptions (Oberkampf *apud* Vaz Jr [2]): (i) the exact solution must be smooth enough that the Taylor series expansion for the error is justified, (ii) the formal convergence order, p, is known, and (iii) the mesh size is sufficiently small such that the leading-order error term dominates the local approximation error, i.e., the convergence is monotonic in the asymptotic range. The exact order of the approximation error is not known a *priori*, which recommends the use of an estimate p^* that can be determined by assuming asymptotic convergence and by applying Eq.(14) to three size nested Cartesian meshes, h_1, h_1, and h_3, which, for a constant refinement ratio, r, yielding

$$e_{h_1} \cong \frac{\varphi_{h_1} - \varphi_{h_2}}{r^{p^*} - 1}, \qquad p^* = \log\left(\frac{\varphi_{h_3} - \varphi_{h_2}}{\varphi_{h_2} - \varphi_{h_1}}\right) \Big/ \log(r) \quad \text{and} \quad r = \frac{h_3}{h_2} = \frac{h_2}{h_1}, \tag{15}$$

where $h_3 > h_2 > h_1$. Errors are evaluated only at coincident nodes for meshes (h_1, h_2 and h_3) and are associated to the most refined mesh h_1, therefore no global *Richardson* measure is computed. In this work *Richardson extrapolation* is used to illustrate the order of error for the displacement calculation. The calculation of the approximate order of the error (p^*) is performed for a simple test case of the a cantilever beam depicted in Fig. 6 for a plane stress problem. In the same test case the monotonic convergence is verified. With the purpose to compare with the analytical solution [2] a slender beam (L/H=20) is employed.

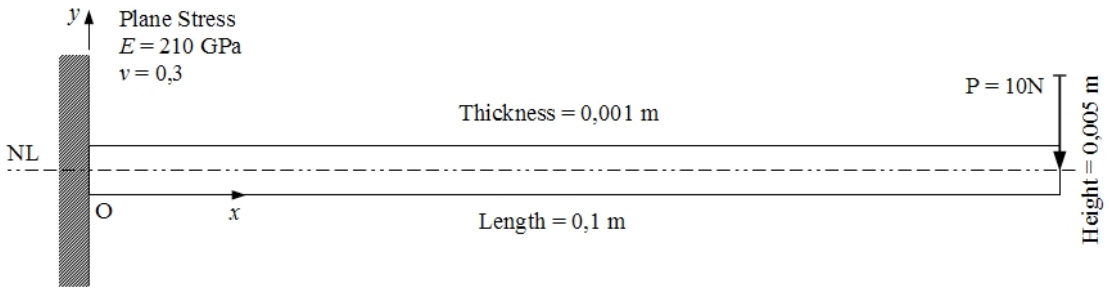

Figure 6: The Cantilever beam used to compute the order p^* and to verify the monotonic convergence.

To verify if the convergence is monotonic, it is used five meshes: 40×2, 80×4, 160×8, 320×16 and 640×32 elements ($N_x \times N_y$). Fig. 7 shows the neutral line near the free end where it can be seen that with the refinement of the mesh the approximate solution tends to the analytical values. Using these results Fig. 8 shows that the convergence is monotonic for a chosen point close to the free end of the neutral line (NL).

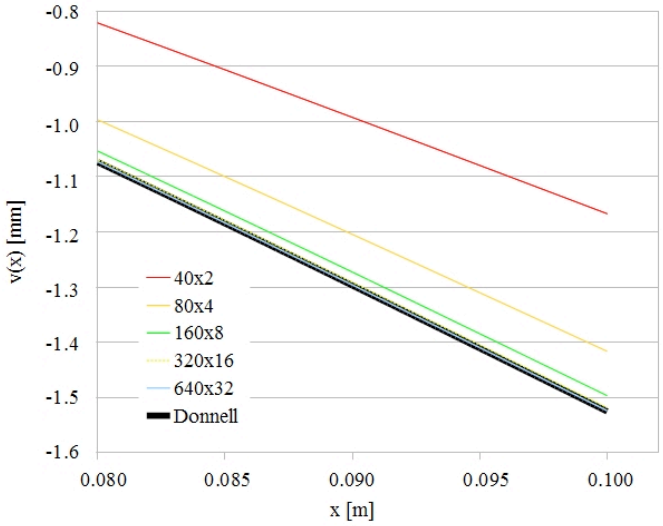

Figure 7: Monotonic convergence for a point near the free end on the neutral line compared with the analytical solution proposed by Donnell.

Order of the error (p^*): The determination of the approximated order of the error is done using Eq.(15) with 640×32 meshes (for h_1), 320×16 (for h_2) and 160×8 (for h_3). The order of the error was obtained for the total displacement *d*, $d$with$= (u^2 + \mathrm{v}^2)^{1/2}$ over the points for the smallest mesh, h_3. The map is shown in Fig. 9. Furthermore the error of *Richardson*, e_h, is also computed and shown in Fig. 10.

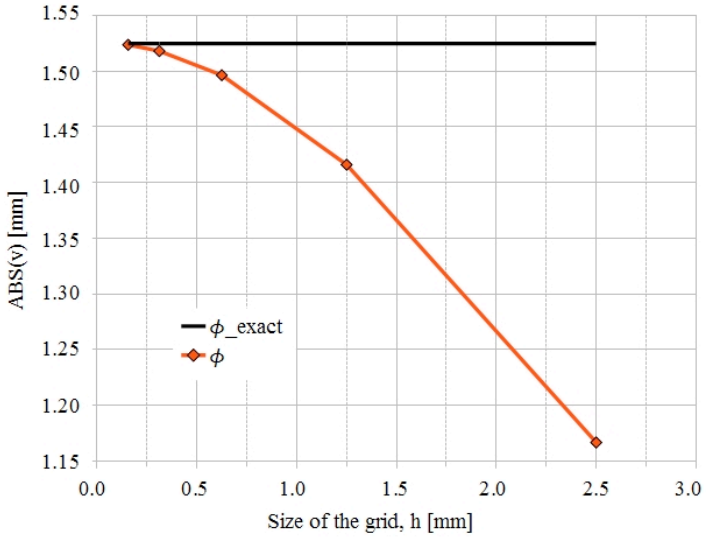

Figure 8: Monotonic convergence for the v displacement of the point (*x*;*y*) = (0,1;0,0025) m.

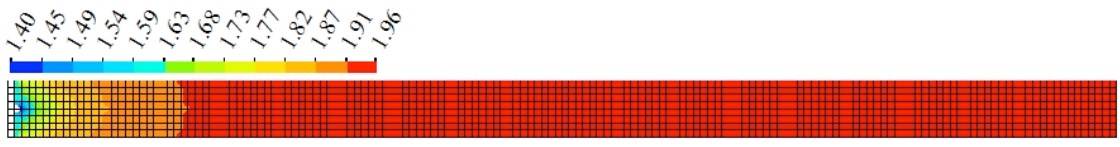

Figure 9: Map of the order of the error (p^*).

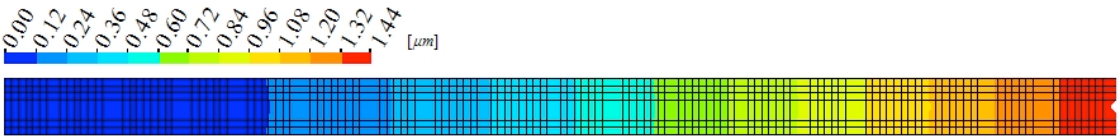

Figure 10: Colour map of the error (e_h) along the beam

Fig. 9 shows that the order of the error is very close to 2.0 over most of the beam, reaching lower values in regions close to the fixed end. Based on these results one can say that the method used is of is of order 2.0. The largest displacements were of the order of 1.5 mm and the greatest errors of the order of 1.44×10^{-3} mm, *i.e.* around 0.1%, indicating a very good approximation. Following, the patch tests are performed in order to check others characteristics of the method.

4.2 Patch Test

The main idea of the Patch Test is to test the discretization method, the computational implementation of the algorithm, the consistency condition and the singularity problem which appears in certain situations. The consistency condition [31] require that in the limit (as h tends to zero) the approximation of Eq.(13) should model exactly the differential equation, Eq. (1). This is of course, minimum requirements, and it is expected to be fulfilled by any numerical method. Regardless the fact that the solution of Eq.(13) was achieved with an error of order $p \geq 2$, the method should reproduce exactly the solution for any linear forms of $\mathbf{u}^*$ as h tends to zero (where h represents the size of the element). For the patch tests *A*, *B*, *C* with single-element, the exact solution presented in Eq.(16) will be used, and for the patch test *C* with slightly degenerated elements, the solution employed is given by Eq.(17). If linear displacements are imposed the resulting analytical stress field are given by

$$\begin{cases} u(x,y) = 0.0014x \\ v(x,y) = 0.0052x + 0.0014y \end{cases} \textit{what produces} \begin{cases} \sigma_{xx} = 2Pa & \sigma_{yy} = 2Pa \\ \sigma_{zz} = 2Pa & \sigma_{xy} = 0 \end{cases} \tag{16}$$

$$\begin{cases} u(x,y) = \ \ 0.0020x \\ v(x,y) = -0.0006y \end{cases} \textit{what produces} \begin{cases} \sigma_{xx} = 2Pa & \sigma_{yy} = 0 \\ \sigma_{zz} = 0 & \sigma_{xy} = 0 \end{cases} \tag{17}$$

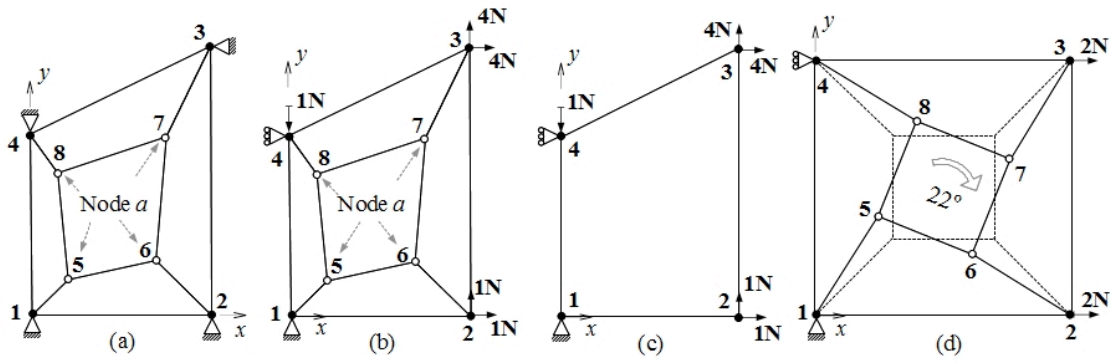

Figure 11: Patch of elements: (a) for patch test *A* and *B*, (b) for patch test *C*, (c) Single-element and (d) patch test *C*, with "degenerated" elements.

Patch Test A: In Test *A*, it is inserted the exact value of the parameters $\mathbf{u}^*$ at the node *a* and it is checked if the identity, given by

$$K_{ij}u_j^* - g_i \equiv 0 \tag{18}$$

for $i = a$, according to Fig.11(a), is verified.

Patch Test B: In Test *B*, only the values of $\mathbf{u}^*$ corresponding to the boundaries of the '*patch*' are inserted and u_a is found through

$$u_i^* = \frac{g_i - (1-\delta_{ij})K_{ij}u_j^*}{\delta_{ij}K_{ij}} \tag{19}$$

for $i = a$, according to Fig.11(a), and compared against the exact value,

Patch Test *C*: In this test, the patch of elements is assembled as before, but subject to prescribed natural boundary conditions. In Eq.(13), fixing only the minimum number of parameters $\mathbf{u}^*$ necessary to obtain a physically valid solution, e.g., eliminating the rigid body motion, a solution is sought for the remaining $\mathbf{u}^*$ values and compared with the exact solution.

Single-element Test: This test is an alternative of test *C*, however, considering a single element. This test is, indeed, a requirement of any good numerical formulation, since a larger patch, possibly, may not reveal the inherent instabilities of a single element.

For comparison, Tab.(2) presents the nodal coordinates, nodal solution and nodal forces given by Eq.(16), referring to Figs.11(a), 11(b) and 11(c) and of Eq.(17) referring to Fig.11(d).

	Eq.(16)						Eq.(17)					
N	x	y	u	v	g_x	g_y	x	y	u	v	g_x	g_y
1	0.0	0.0	0.0	0.0	-4.0	-4.0	0.0	0.0	0.0	0.0	-2.0	0.0
2	2.0	0.0	0.0028	0.0104	1.0	1.0	2.0	0.0	0.004	0.0	2.0	0.0
3	2.0	3.0	0.0028	0.0146	4.0	4.0	2.0	2.0	0.004	-0.0012	2.0	0.0
4	0.0	2.0	0.0	0.0028	-1.0	-1.0	0.0	2.0	0.0	-0.0012	-2.0	0.0
Figs.11(a) and 11(b)												
5	0.4	0.4	0.00056	0.00264	0.0	0.0	0.48	0.78	0.000959	-0.000467	0.0	0.0
6	1.4	0.6	0.00196	0.00812	0.0	0.0	1.22	0.48	0.002442	-0.000288	0.0	0.0
7	1.5	2.0	0.00210	0.0106	0.0	0.0	1.52	1.22	0.003041	0.000733	0.0	0.0
8	0.3	1.6	0.00042	0.0038	0.0	0.0	0.78	1.52	0.001558	-0.000912	0.0	0.0

Table 2: Nodal coordinates, solution and forces, Eq.(16), Fig.(11a, b, c) and Eq.(17), Fig.11(d).

Test A: Using Fig. 11(a) and the solution given by Eq.(16), assign to the border nodes the analytical values of Tab.(2), getting a system of equations. Use Eq. (18) for nodes 5, 6, 7 and 8 obtaining the residues g_x and g_y given in Tab.(3). It can be seen that the

residues are of the order of the truncation errors, what indicates a good behavior of the method in this test.

	Test A		*Test B*		*Test C*			
N	g_x	g_y	u^*	v*	u^*	error	v*	error
2					0.00280	1.04E-17	0.0104	9.89E-17
3					0.00280	3.99E-17	0.0146	9.71E-17
4							0.0028	2.04E-17
5	-1.75E-15	-3.33E-15	5.60E-04	2.64E-03	0.00056	0.0	0.00264	9.97E-18
6	3.77E-15	-4.86E-14	1.96E-03	8.12E-03	0.00196	0.0	0.00812	3.99E-17
7	-1.56E-14	1.05E-13	2.10E-03	1.06E-02	0.00210	1.95E-17	0.01060	9.71E-17
8	-3.33E-15	0.00E+00	4.20E-04	3.80E-03	0.00042	3.04E-18	0.00380	1.99E-17

Table 3: *Test A* – Residues g_x and g_y. *Test B* – Displacements u and v. *Test C* – Displacement u and v with respective errors.

Test B: As in test A, using Fig.11(a) and the solution given by Eq.(16), it is assigned to the boundary nodes the analytical values of Tab.2. Eq. (19) is then applied to nodes 5, 6, 7 and 8 resulting in the values for the displacements u^* and v* given by Tab. 3. The values obtained coincide exactly with the analytical values of the Tab.2. This demonstrates that the method behaved correctly also in the calculation of the displacement.

Test C: Now using Fig.11(b) and the solution given by Eq.(16), it is assigned to the boundary nodes analytical values of Tab.(2) to the for displacements and forces. Then Eq. (19) is applied for nodes 2, 3, 5, 6, 7 and 8 for u and v displacements and v displacement only to node 4, obtaining the values for the displacements u^* and v* given in Tab.(3) with their absolute errors. Again the errors obtained fall in the range of the truncation errors of the calculation.

Single-element: Using Fig.11(c) and the solution given by Eq. (16), it is assigned to the boundary nodes the analytical values found in Tab.(2) for prescribed displacements and forces. Now using Eq. (19) for nodes 2 and 3 for u and v and to node 4 only for v displacement, the values for the displacements u^* and v* are obtained. Again, the numbers coincide with the analytical ones.

Test C with "degenerated" elements: Using Fig.11(d) and the solution given by Eq.(17), it is assigned to the boundary nodes the analytical values found in Tab.(2) for displacements and forces. Then Eq. (19) is applied for nodes 2, 3, 5, 6, 7 and 8 for u and v and to node 4 only for v displacement, obtaining the values for the displacements u^* and v* that exactly match the analytical values of the tab.(2).

4.3 Convergence behavior of the linear system

Eq.(13), in many situations, needs solved by iterative methods. No efforts were made in order to use more efficient solvers. In spite of that, in this section, an analysis of the convergence rate of the solution using Gauss-Seidel with and without *Successive Over-Relaxation* (SOR) is performed. The iterative process is stopped when the norm of the residue reaches certain level of tolerance, with the norm ($\|\mathbf{R}\|$) calculated using

Eq.(20). The initial values are zeros for all $\mathbf{u}^*$. The problem test used in this evaluation is presented in Fig. 12. In Fig.12 the geometry, boundary conditions and the map for the displacement u^* are shown.

$$R = \sqrt{\sum_{i=1}^{n_{eq}} (R_i)^2} \tag{20}$$

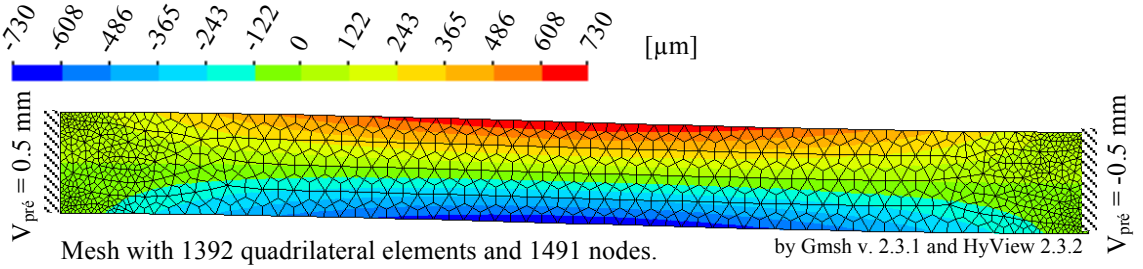

Figure 12: Geometry, boundaries conditions and displacement map.

Fig. 13 shows the number of iterations as a function of the acceleration parameter, indicating that the value of 1.82 was the best coefficient for this problem. Recall that this coefficient depends on the grid used.

$$\left(\phi_P^{I+1}\right)_{SOR} = \omega\left(\phi_P^{I+1}\right)_{Gauss-Seidel} + (\omega - 1)\phi_P^I \tag{21}$$

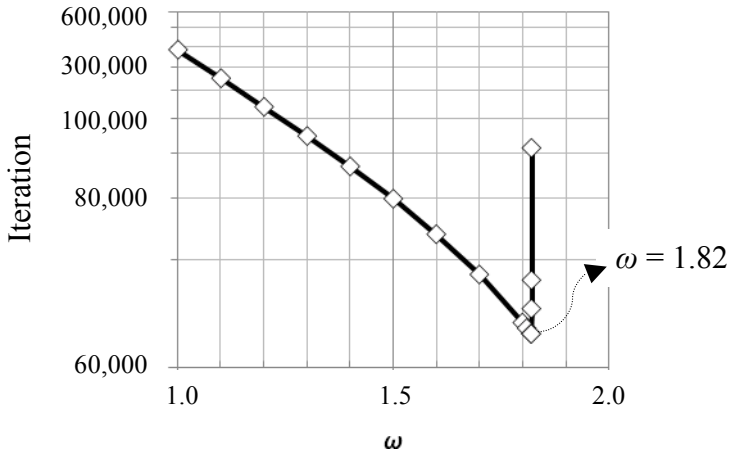

Figure 13: Relaxation coefficient ω for the problem illustrated in Fig.12.

Finally, in order to verify the computational gains using SOR, Fig. 14 shows the number of iteration using Gauss-Seidel and S.O.R with the optimum relaxation coefficient. It can be seen the enormous reduction in the number iteration when the optimum parameter is used, from 450.000 to 75.000 iterations.For both methods the convergence is smooth and well behaved.

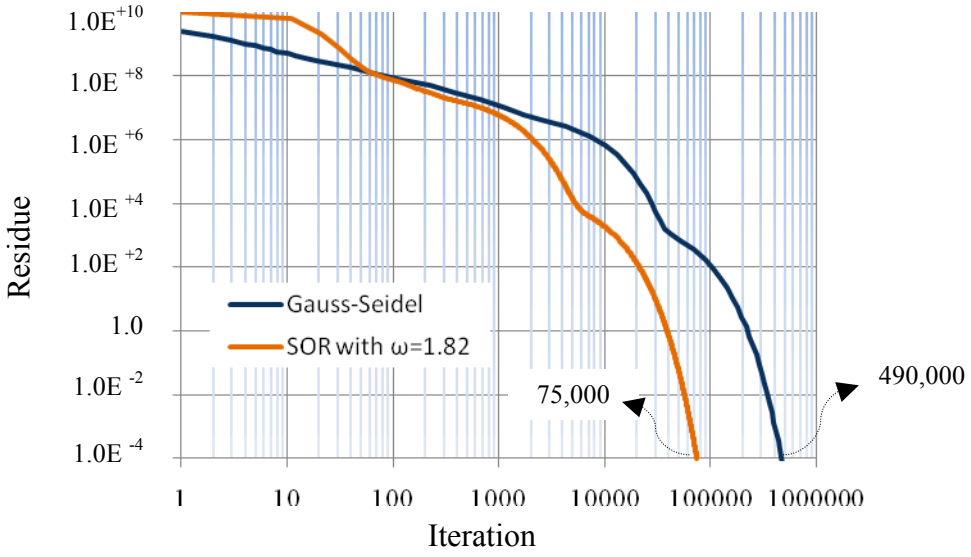

Figure 14: Convergence rate of the norm $\|\mathbf{R}\|$.

The convergence of the norm of the residue is smooth for both solution methods. Initially the SOR showed higher residue, but until this iteration 100 was lower than the residue obtained in the Gauss-Seidel. Finally the methods converge to the tolerance adopted ($Tol = 1\times10^{-4}$) with 490,000 iterations for Gauss-Seidel and 75,000 iterations for SOR method, that is, only 15% of that.

5 CONCLUSIONS

Following, some conclusions are drawn from the results obtained with the tests made for evaluating the EbFVM presented in this paper.

5.1 Richardson extrapolation

The application of Richardson error analysis is valid for situations in which the convergence of the solution according to the size of the mesh (h) is monotonic, and this was verified for the case considered, as shown in Fig. 8.

The order of the error tends to be of close to 2 for most of the domain, as reported in Fig. 9. In a similar case (double-clamped cantilever beam) and using the classic finite volume method on a grid Cartesian, Vaz Jr [2] analyzed the order of the error for both the displacements and stresses, and also obtained close to 2.0.

Errors in displacement are small throughout the beam, reaching maximum values of 1.44×10^{-3} mm in the free edge and values of the order 10^{-4} mm in most of the domain, according to Fig. 10. The largest displacements is of the order of 1.5 mm and the largest errors 1.44×10^{-3} mm, *i.e.* error of the order of 0.1%.

5.2 Patch tests

The method has demonstrated good behavior in all proposed tests: *Test A*, *Test B*, *Test C*, *Single-element test* and *Test C* with "degenerated" elements. This permits to say that asymptotic convergence is ensured, the algorithm is robust, the solution continuity between elements is ensured and that the algorithm was correctly implemented.

5.3 Assembling technique

The sweeping of the domain element-by-element, renders to developed method generality in dealing with any type of grid and the necessary tools for easy implementation in existing fluid flow and finite element codes.

5.4 Concluding remarks

The results obtained herein reinforce the statements already found in the literature that finite volume methods are suitable for solving solid mechanics problems. The method presented contains all the ingredients required for a general method, like unstructured grids with suitable computational abstraction for implementing element or edge based methods. Associated to these features, the conservative principle at discrete level confers to the method stability and robustness. Coupled problems seems to be the major application for the technology advanced in this work.

REFERENCES

[1] Alejandro C. Limache and Sergio R. Idelsohn, On the Development of Finite Volume Methods for Computational Solid Mechanics. *Asociación Argentina de Mecânica Computacional - Mecânica Computacional- Córdoba-Argentina*, **26**, pp. 827-843 (2007)

[2] Miguel Vaz Jr, Pablo Andrés Muñoz-Rojas and Gerson Filippini, On the Accuracy of Nodal Stress Computation in Plane Elasticity using Finite Volumes and Finite Elements. *Computers and Structures*, **87**, pp. 1044-1057 (2009)

[3] Y.D. Fryer, C. Bailey, M. Cross and C.H. Lai, A Control Volume Procedure for Solving the Elastic Stress-strain Equations on an Unstructured Mesh. *Journal: Applied Mathematical Modelling*, **15**, pp. 639-645 (1991)

[4] J. Fainberg and H.J. Leister, Finite Volume Multigrid Solver for Thermo-Elastic Stress Analysis in Anisotropic Materials. *Computer Methods in Applied Mechanics and Engineering*, **137**, pp. 167-174 (1996)

[5] E. Oñate, M. Cervera, O.C. Zienkiewicz, A Finite Volume Format for Structural Mechanics. *International Journal for Numerical Methods in Engineering*, **37**, pp. 181-201 (1994)

[6] C. Bailey and M. Cross, A Finite Volume Procedure to Solve Elastic Solid Mechanics Problems in Three Dimensions on an Unstructured Mesh. *International Journal for Numerical Methods in Engineering*, **38**, pp. 1757-1776 (1995)

[7] G.A. Taylor, C. Bailey and M. Cross, Solutions of the Elastic/Visco-Plastic Constitutive Equations: A Finite Volume Approach. *Applied Mathematical Modeling*, **19**, pp. 746-760 (1995)

[8] M.A. Wheel, A Finite-Volume Approach to the Stress Analysis of Pressurized Axisymmetric Structures. *International Journal Pressure Vessel & Piping*, **68**, pp. 311-317 (1996)

[9] M.A. Wheel, A Finite-Volume Method for Analysing the Bending Deformation of Thick and Thin Plates. *Computer Methods in Applied Mechanics and Engineering*, **147**, pp. 199-208 (1997)

[10] M.A. Wheel, Modelling Incompressible Materials Using a Mixed Structural Finite Volume Approach. *5th ACME Conference – Computational mechanics in UK*, Londres-UK, pp. 32-35, (1997)

[11] M.A. Wheel, Further Observations on Modeling Incompressible Materials Using a Finite Volume Approach. *6th ACME Conference – Computational mechanics in UK*, Exeter-UK, pp. 43-46, (1998)

[12] K. Zarrabi and A. Basu, A Finite Volume Element Formulation for Solution of Elastic Axisymmetric Pressurized Components. *International Journal of Pressure Vessels and Piping*. **77**, pp. 479-484, (2000)

[13] I. Demirzic, I. Horman and D. Martinovic, Finite Volume Analysis of Stress and Deformation in Hygro-Thermo-Elastic Ortotropic Body. *Computer Methods in Applied Mechanics and Engineering*, **190**, pp. 1221-1232 (2000)

[14] A.K. Slone, K. Pericleous, C. Bailey and M. Cross, Dynamic Fluid-Structure Interaction Using Finite Volume Unstructured Mesh Procedures. *Computer & Structures*, **80**, pp. 371-390 (2002)

[15] Gareth A. Taylor, Michael Hughes, Nadia Strusevich, Koulis Pericleous, Finite Volume Methods Applied to the Computational Modelling of Welding Phenomena. *Applied Mathematical Modelling*, **26**, pp. 309-320 (2002)

[16] A.J. Williams, T.N. Croft and M. Cross, Computational Modeling of Metal Extrusion and Forging Processes. *Journal of Materials Processing Technology*, **125**, pp. 573-582 (2002)

[17] Gerson Filippini, O Método de Volumes Finitos Aplicado A Elasticidade Plana em Material Isotrópico. Dissertação de Mestrado em Ciência e Engenharia de Materiais - *Universidade do Estado de Santa Catarina-UDESC*, Joinville-SC-Brasil, p. 108 (2004)

[18] O.C. Zienkiewicz and E. Oñate, Finite Volumes vs Finite Elements is There Really a Choice? *International Center for Numerical Methods in Engineering*, **8** (1990)

[19] Andreas Lahrmann, An Element Formulation for the Classical Finite Difference and Finite Volume Method Applied to Arbitrarily Shaped Domains. *International Journal for Numerical Methods in Engineering*, **35**, pp. 893-913 (1992)

[20] S.R. Idelsohn, and E. Oñate, Finite Volumes and Finite Elements: Two "Good Friends". *International Journal for Numerical Methods in Engineering*, **37**, pp. 3323-3341 (1994)

[21] C. Bailey, G. Taylor, S.M. Bounds, G. Moran and M. Cross, PHYSICA: A Multiphysics Computational Framework and its Application to Casting Simulations. *Computational Fluid Dynamics in Mineral & Metal Processing and Power Generation*, London - UK, pp. 419-425 (1997)

[22] G.A. Taylor, C. Bailey and M. Cross, Computational Solid Mechanics Using a Vertex-Based Finite Volume Method. *In F. Benkhaldoun and D. Hanel, editors, Finite Volumes for Complex Applications II: Problems and Perspectives*, pp. 507-515 (1999)

[23] N.A. Fallah, C. Bailey, M. Cross, G.A. Taylor. Comparison of Finite Element and Finite Volume Methods Application in Geometrically Nonlinear Stress Analysis. *Applied Mathematical Modelling*, **24**, pp. 439-455 (2000)

[24] Tetsuro Yamamoto, Qing Fang, and Takuya Tsuchiya, Finite Difference, Finite Element and Finite Volume Methods Applied to Two-Point Boundary Value Problems. *Journal of Computational and Applied Mathematics*, **139**, pp. 9-19 (2002)

[25] M.A. Wheel and P. Wenke, A Finite Volume Method for Solid Mechanics Incorporating Rotational Degrees of Freedom. *Computers & Structures*, **81**, pp. 321-329 (2003)

[26] A.K. Slone, C. Bailey and M. Cross, Dynamic Solid Mechanics Using Finite Volume Methods. *Applied Mathematical Modeling*, **27**, pp. 69-87 (2003).

[27] G.H. Xia, Y. Zhao, J.H. Yeo, X. Lv, A 3D Implicit Unstructured-Grid Finite Volume Method for Structural Dynamics. *Computational Mechanics*, **40**, pp. 299-312 (2007)

[28] Y. Zhao, X. Lv, X.Y. Huang, G.H. Xia, X.H. Su, A Matrix-Free Implicit Unstructured Multigrid Finite Volume Method for Simulating Structural Dynamics and Fluid-Structure Interation. *Journal of Computational Physics*. **225**, pp. 120-144 (2007)

[29] Alejandro C. Limache and Sergio R. Idelsohn, On the Development of Finite Volume Methods for Computational Solid Mechanics. *Asociación Argentina de Mecânica Computacional - Mecânica Computacional*, Córdoba-Argentina, **26**, pp. 827-843 (2007)

[30] Ian Craw, Advanced Calculus and Analysis MA1002 University of Aberdeen, *Department of Mathematical Sciences*, (2000)

[31] O.C. Zienkiewicz, R.L. Taylor and J.Z. Zhu, The Finite Element Method: Its Basis and Fundamentals. New Yourk: Elsevier: 733 p. (2006)